Volume 4
Number 24
21 December 2022
Pages 5193–5418

Nanoscale Advances

rsc.li/nanoscale-advances

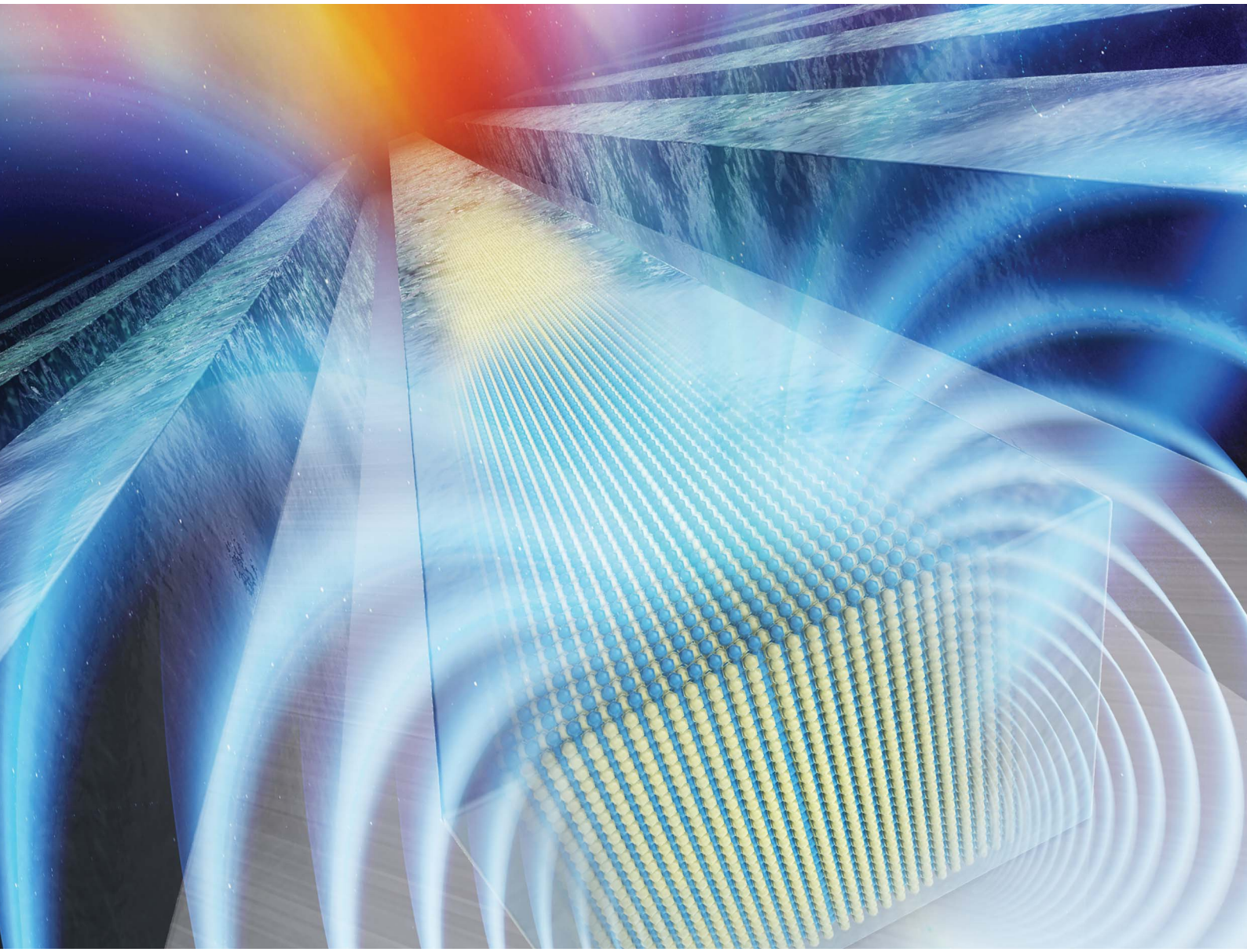

ISSN 2516-0230

ROYAL SOCIETY OF CHEMISTRY

PAPER
Yutaka Majima *et al.*
Nanostructure-induced $L1_0$-ordering of twinned single-crystals in CoPt ferromagnetic nanowires

NCNST

Nanoscale Advances

ROYAL SOCIETY OF CHEMISTRY

PAPER

View Article Online
View Journal | View Issue

Cite this: *Nanoscale Adv.*, 2022, **4**, 5270

Nanostructure-induced $L1_0$-ordering of twinned single-crystals in CoPt ferromagnetic nanowires†

Ryo Toyama, [a] Shiro Kawachi, [bcd] Jun-ichi Yamaura, [bc] Takeshi Fujita, [e] Youichi Murakami,[c] Hideo Hosono[b] and Yutaka Majima *[ab]

$L1_0$-ordered ferromagnetic nanowires with large coercivity are essential for realizing next-generation spintronic devices. Ferromagnetic nanowires have been commonly fabricated by first $L1_0$-ordering of initially disordered ferromagnetic films by annealing and then etching them into nanowire structures using lithography. If the $L1_0$-ordered nanowires can be fabricated using only lithography and subsequent annealing, the etching process can be omitted, which leads to an improvement in the fabrication process for spintronic devices. However, when nanowires are subjected to annealing, they easily transform into droplets, which is well-known as Plateau–Rayleigh instability. Here, we propose a concept of "nanostructure-induced $L1_0$-ordering" of twinned single-crystals in CoPt ferromagnetic nanowires with a 30 nm scale ultrafine linewidth on Si/SiO_2 substrates. The driving forces for nanostructure-induced $L1_0$-ordering during annealing are atomic surface diffusion and extremely large internal stress at ultrasmall 10 nm scale curvature radii of the nanowires. $(Co/Pt)_6$ multilayer nanowires are fabricated by a lift-off process combining electron-beam lithography and electron-beam evaporation, followed by annealing. Cross-sectional scanning transmission electron microscope images and nano-beam electron diffraction patterns clearly indicate nanostructure-induced $L1_0$-ordering of twinned single-crystals in the CoPt ferromagnetic nanowires, which exhibit a large coercivity of 10 kOe for perpendicular, longitudinal, and transversal directions of the nanowires. Two-dimensional grazing incidence X-ray diffraction shows superlattice peaks with Debye–Scherrer ring shapes, which also supports the nanostructure-induced $L1_0$-ordering. The fabrication method for nanostructure-induced $L1_0$-ordered CoPt ferromagnetic nanowires with twinned single-crystals on Si/SiO_2 substrates would be significant for future silicon-technology-compatible spintronic applications.

Received 14th September 2022
Accepted 6th October 2022

DOI: 10.1039/d2na00626j

rsc.li/nanoscale-advances

1. Introduction

Ferromagnetic nanowires have great potential for ultrahigh-density data storage applications, such as magnetic domain-wall racetrack memory and perpendicular magnetic recording,[1–9] as well as for spintronic sensors,[10–17] spin torque oscillators,[18,19] excitation of spin waves,[20,21] spinmotive force devices,[22,23] and biomedical applications.[24,25] In magnetic domain-wall racetrack memory, magnetic domains in an array of ferromagnetic nanowires store the data.[1–6] Multilayered nanowires with ferromagnetic and non-magnetic layers such as Co/Cu can be used as spintronic sensors based on giant magnetoresistance effect.[10–16] Magnetostrictive sensors based on Co nanowires on flexible substrates have also been demonstrated.[17]

In particular, ferromagnetic materials with strong perpendicular magnetocrystalline anisotropy and large coercivity (H_c) are necessary for the nanostructures to be immune to the thermal fluctuation of magnetization above room temperature.[26,27] From this perspective, $L1_0$-ordered alloys such as CoPt are considered to be promising candidates, where $L1_0$-ordering of CoPt is obtained through the phase transformation from the $A1$-disordered phase by thermal treatment.[28–31]

To fabricate $L1_0$-CoPt, epitaxial growth technique and management of lattice-mismatch-induced strain on single-crystal insulating substrates such as MgO(001) have been widely utilized.[32,33] Combining these with annealing allows for a facile fabrication of perpendicularly-magnetized tetragonal $L1_0$-CoPt films possessing alternating monoatomic layers of Co

[a]*Laboratory for Materials and Structures, Institute of Innovative Research, Tokyo Institute of Technology, Yokohama, Kanagawa 226-8503, Japan. E-mail: majima@msl.titech.ac.jp*

[b]*Materials Research Center for Element Strategy, Tokyo Institute of Technology, Yokohama, Kanagawa 226-8503, Japan*

[c]*Institute of Materials Structure Science, High Energy Accelerator Research Organization (KEK), Tsukuba, Ibaraki 305-0801, Japan*

[d]*Graduate School of Science, University of Hyogo, Kamigori, Hyogo 678-1297, Japan*

[e]*School of Environmental Science and Engineering, Kochi University of Technology, Kami, Kochi 782-8502, Japan*

† Electronic supplementary information (ESI) available: SEM images of CoPt nanowires after annealing at 650 °C for 30 and 60 min; 2D GI-XRD patters of CoPt nanowires after annealing at 650 °C for 30 and 60 min. See https://doi.org/10.1039/d2na00626j

and Pt towards the direction normal to the substrates.[32,33] Moreover, the $L1_0$-ordering has reportedly been enhanced by rapid thermal annealing (RTA), where the in-plane tensile stress between ferromagnetic thin film and substrate, which is induced by the high heating rate of RTA, contributed to the high degree of $L1_0$-ordering.[34–42] After fabricating $L1_0$-CoPt thin films based on these growth techniques, nanowire structures have been commonly prepared using lithography and finally etching the ordered films.[43]

Recently, we have developed a fabrication process for Pt-based nanogap electrodes by a lift-off process that combines electron-beam lithography (EBL) and electron-beam (EB) evaporation.[44–49] Pt-based nanogap electrodes with an ultrafine linewidth of 10 nm were successfully fabricated by optimizing the fabrication conditions.[44]

We also reported the $L1_0$-ordering of Co/Pt multilayer thin films on thermally oxidized Si (Si/SiO_2) substrates by EB evaporation and annealing processes, which was characterized by scanning electron microscope (SEM), grazing incidence X-ray diffraction (GI-XRD), and vibrating sample magnetometer (VSM).[50–52] In Pt (6.6 nm)/Co (4.8 nm) bilayer thin films, graded films consisting of $L1_2$-ordered $CoPt_3$, $L1_0$-CoPt, and $L1_2$-ordered Co_3Pt were formed during interdiffusion of the bilayer annealed at 800 °C for 30 s by RTA in a vacuum.[50] Because the interdiffusion and $L1_0$-ordering of CoPt were in progress owing to the short annealing time of 30 s RTA process and both $L1_2$-$CoPt_3$ and $L1_2$-Co_3Pt do not usually show large H_c, an H_c in the graded films was as small as 2.1 kOe.[50] In [Co (1.2 nm)/Pt (1.6 nm)]$_4$ multilayer thin films, isolated round grains of single-phase $L1_0$-CoPt were formed after annealing in a vacuum at 900 °C for approximately 60 min, which exhibited an improved H_c of 2.7 kOe due to the sufficient interdiffusion by multilayered structure and extended annealing time.[51] Moreover, we also showed that hydrogen annealing contributed to the enhanced H_c of $L1_0$-CoPt.[52] After annealing of the $(Co/Pt)_4$ multilayer thin films at 800 °C for 60 min, a maximum H_c of 13.3 kOe was obtained in $L1_0$-CoPt, which exhibited angular-outline isolated grain structures.[52]

If the nanowires can be directly fabricated Si/SiO_2 substrates by first using lithography and then $L1_0$-ordering of initially disordered ferromagnetic films by annealing, the etching process can be omitted, which leads direct fabrication process of spintronic devices on Si/SiO_2 substrates. Direct fabrication of $L1_0$-CoPt nanowires on Si/SiO_2 substrates using only lithography and subsequent annealing can be beneficial for the future integration of non-volatile spintronics with silicon-technology-based complementally metal-oxide semiconductor (CMOS) integrated circuits.[53,54] This integration will pave the way for the realization of CMOS-compatible multifunctional nanodevices utilizing both the charge and spin of an electron.[55–59]

To achieve the fabrication of $L1_0$-CoPt nanowires on Si/SiO_2 substrates, two challenges remain: the establishment of a fabrication process for CoPt ferromagnetic nanowires with linewidths less than a few tens of nanometers and the $L1_0$-ordering process of CoPt nanowires on Si/SiO_2 substrates. For integrated spintronic device applications, the linewidth of ferromagnetic nanowires is preferably as narrow as possible. Several fabrication processes for ferromagnetic nanowires have been reported, such as etching, electrodeposition, focused-electron-beam-induced deposition, and lift-off processes.[43,60–63] $L1_0$-FePt nanowires with linewidths ranging from 2 μm to 30 nm have been fabricated by first depositing 10 nm-thick $L1_0$-FePt layer on single-crystal MgO(001) substrates and then etching by means of EBL and ion milling techniques.[63] Electrodeposition on anodized aluminum oxide templates have yielded perpendicularly aligned $L1_0$-CoPt nanowires with diameters of 20–200 nm and some of these nanowires exhibited a large H_c over 10 kOe.[64–73]

However, in nanostructures below a few tens of nanometers, there is an extremely large internal stress, which is inversely proportional to the 10 nm-scale curvature radii and proportional to the surface tension, according to Young–Laplace equation given by:[74–76]

$$\Delta P = \gamma\left(\frac{1}{R_1} + \frac{1}{R_2}\right) \quad (1)$$

Here, ΔP is the pressure difference across the surface, γ is the surface tension, and R_1 and R_2 are the principal radii of surface curvature.[74–76] When nanowires are subjected to annealing, they can easily transform into droplet structures by atomic surface diffusion so as to minimize the surface free energy,[77–84] which is well-known as Plateau–Rayleigh instability.[85–90] The structural deformation by Plateau–Rayleigh instability upon annealing limits a reproducible fabrication of nanowire structures with linewidths below a few tens of nanometers on solid-state substrates. In addition, the $L1_0$-ordering process of CoPt nanowires on Si/SiO_2 substrates should also be established. However, $L1_0$-ordering of CoPt on amorphous SiO_2 substrate surfaces has been challenging because the epitaxial growth technique or lattice-mismatch-induced strain cannot be utilized for the growth of $L1_0$-CoPt.[34] Therefore, the direct fabrication method of position-defined $L1_0$-CoPt nanowires with narrow linewidths and a large H_c on Si/SiO_2 substrates is yet to be reported.

In this paper, we propose a concept of "nanostructure-induced $L1_0$-ordering" of twinned single-crystals in CoPt ferromagnetic nanowires with a 30 nm scale ultrafine linewidth on Si/SiO_2 substrates, where the atomic interdiffusion, surface diffusion, and extremely large internal stress at ultrasmall 10 nm scale curvature radii of the nanowires during annealing are the driving forces for nanostructure-induced $L1_0$-ordering. The ordering mechanism in the nanowires in this study is different from previous studies. Nanostructure-induced $L1_0$-ordering of CoPt ferromagnetic nanowires would be realized by fabricating CoPt nanowires with a 30 nm scale narrow linewidth on Si/SiO_2 substrates using only lithography and utilizing annealing. We demonstrate the proof-of-concept of nanostructure-induced $L1_0$-ordering method for fabricating twinned single-crystals in CoPt ferromagnetic nanowires on Si/SiO_2 substrates by a lift-off process combining EBL and EB evaporation, followed by annealing. The surface morphologies, crystal structures, magnetic properties, and cross-sectional profiles of the nanowires are analyzed by SEM, GI-XRD, VSM, and transmission electron microscope (TEM), respectively.

2. Results and discussion

Fig. 1 shows typical top-view SEM images of the CoPt nanowires before and after annealing at 650 °C for 90 min. The annealed nanowires showed linewidths of 20–30 nm without disconnection of the nanowire structures (Fig. 1b). Linewidth perturbation was also observed for the annealed nanowires (Fig. 1b). Moreover, Fig. S1† shows the SEM images of the CoPt nanowires after annealing for 30 and 60 min, which also exhibited nanowire structures without disconnection after annealing.

The two-dimensional (2D) GI-XRD pattern of the CoPt nanowires after annealing at 650 °C for 90 min is shown in Fig. 2. The pattern was obtained by subtracting the background signal of Si/SiO_2 substrates from the pattern of the nanowires on the substrates. From the subtracted 2D GI-XRD pattern (Fig. 2), superlattice peaks of $L1_0$-CoPt *001* and *110* were clearly observed, indicating the $L1_0$-ordering of the CoPt nanowires after annealing. The peak shapes of $L1_0$-CoPt *001* and *110* were Debye–Scherrer rings (Fig. 2), which indicates that the *c*-axis of $L1_0$-CoPt tended to be oriented perpendicular to the curved surface of the nanowires. Moreover, the other superlattice peaks of $L1_0$-CoPt *201* and *112* and the fundamental peaks of *111*, *220*, and *311* were also clearly observed (Fig. 2). The nanostructure induced $L1_0$-ordering of the nanowires was also confirmed after annealing for 30 and 60 min, as evident in the superlattice peaks of $L1_0$-CoPt *001* and *110* with Debye–Scherrer ring shapes (Fig. S2†). The intensity of the $L1_0$-CoPt *001* peak of the nanowires became stronger for longer annealing times (Fig. S2†). On the other hand, the full-width at half maximum of $L1_0$-CoPt *001* became smaller for longer annealing times (Fig. S2†).

The intensity–2θ one-dimensional (1D) GI-XRD profiles of the CoPt nanowires after annealing at 650 °C for 90 min are shown in Fig. 3. The 2θ values for $L1_0$-CoPt *001* and *110* were 16.450° and 22.722°, respectively. Therefore, the *c* and *a* values for the $L1_0$-CoPt nanowires were determined to be $c = 3.6804$ Å and $a = 3.7799$ Å, respectively, which agrees with values in the literature.[32,50–52,68,70,91]

The magnetic hysteresis loops (*M*–*H* curves) of the nanowires after annealing at 650 °C for 90 min are shown in Fig. 4. The H_c of the annealed nanowires in the transversal ($H_{c\perp}$), longitudinal ($H_{c\parallel}$), and perpendicular ($H_{c\perp}$) directions were 10.6, 10.7, and 10.8 kOe, respectively, which indicates that the nanowires showed an identical H_c value for the three measured directions (Fig. 4).

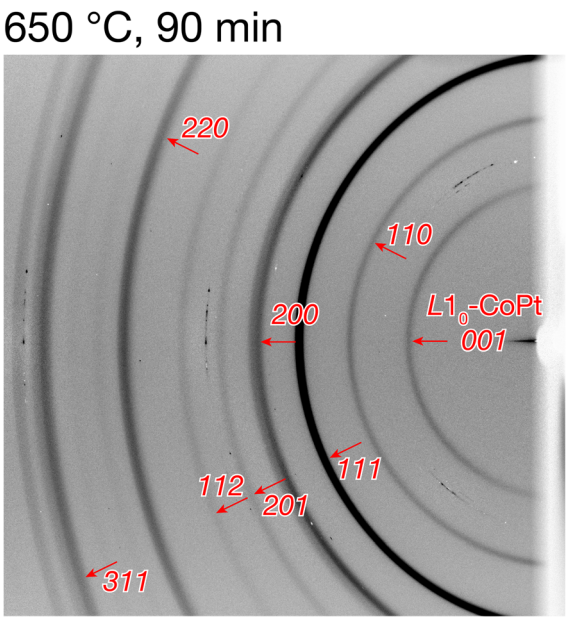

Fig. 2 Two-dimensional (2D) grazing incidence X-ray diffraction (GI-XRD) pattern of $(Co/Pt)_6$ nanowires on Si/SiO_2 substrates after annealing at 650 °C for 90 min. The diffraction peaks of $L1_0$-CoPt (*001*, *110*, *111*, *200*, *201*, *112*, *220*, and *311*) are indicated by red arrows. The 2D GI-XRD patterns of the nanowires after annealing at 650 °C for 30 and 60 min are shown in Fig. S2.†

Fig. 5 shows the cross-sectional bright field (BF)-TEM images, high-angle annular dark field (HAADF)-scanning transmission electron microscope (STEM) images, and nanobeam electron diffraction (NED) pattern of the CoPt nanowires after annealing at 650 °C for 90 min, which were observed from the nanowire-axis direction along the [110] zone axis. The nanowires exhibited elliptical cross-sectional shapes with reduced heights compared to the initial total thickness of 50.4 nm (Fig. 5a, b and d). From the NBD pattern (Fig. 5c),

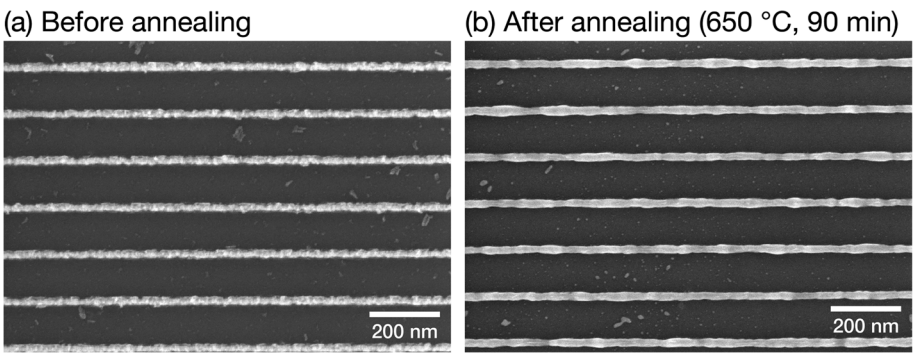

Fig. 1 Typical top-view scanning electron microscope (SEM) images of [Co (3.6 nm)/Pt (4.8 nm)]$_6$ multilayer nanowires on Si/SiO_2 substrates (a) before and (b) after annealing at 650 °C for 90 min. The SEM images of CoPt nanowires after annealing at 650 °C for 30 and 60 min are shown in Fig. S1.†

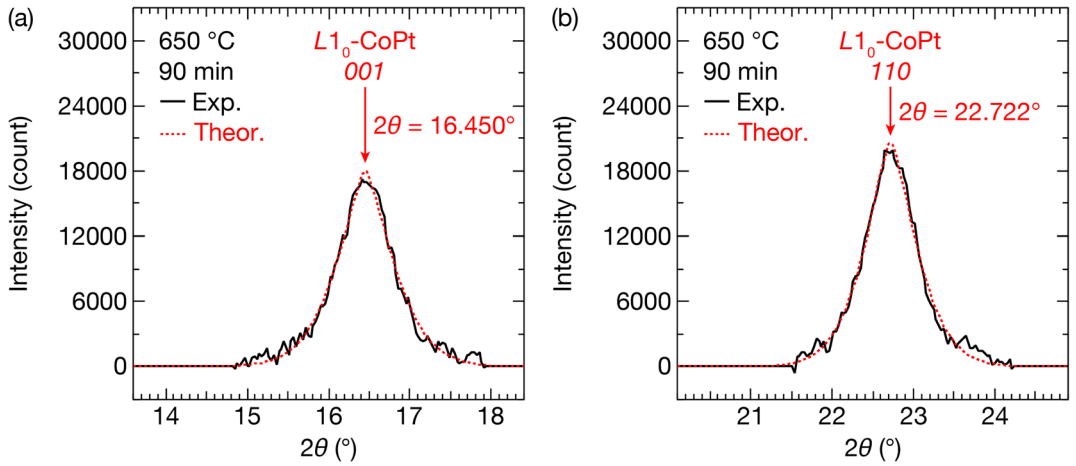

Fig. 3 Intensity–2θ 1D GI-XRD profiles of $(Co/Pt)_6$ nanowires on Si/SiO_2 substrates after annealing 650 °C for 90 min. Each of the experimental peaks (black curve) of (a) $L1_0$-CoPt *001* and (b) $L1_0$-CoPt *110* was analyzed by a bell-shaped function after subtracting the remaining background signal. These theoretical curves are plotted as red dotted curves.

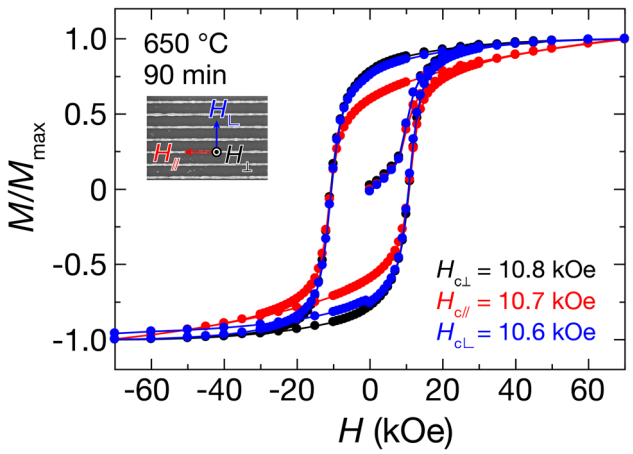

Fig. 4 Magnetic hysteresis loops (M–H curves) of $(Co/Pt)_6$ nanowires on Si/SiO_2 substrates after annealing at 650 °C for 90 min. M–H curves were measured in a vacuum at room temperature (27 °C) by applying a magnetic field in the out-of-plane direction (perpendicular; black curves and filled circles), in-plane direction parallel to the nanowire-axis (longitudinal; red curves and filled circles), and in-plane direction perpendicular to the nanowire-axis (transversal; blue curves and filled circles). $H_{c\perp}$, $H_{c\parallel}$, and $H_{c\perp}$ represent H_c for perpendicular, longitudinal, and transversal directions, respectively.

superlattice diffraction spots of $L1_0$-CoPt *001* and *110* (indicated by the red circles) were observed along with the fundamental spots (indicated by the yellow circles), which indicates $L1_0$-ordering of the CoPt nanowires after annealing. From the magnified HAADF-STEM images, alternating monoatomic layers of Co (appeared as dark spots and indicated by the light blue dots) and Pt (appeared as bright spots and indicated by the orange dots) were clearly observed along the [110] zone axis at the top-edge of the nanowires (Fig. 5e) and near the nanowire–substrate interface (Fig. 5f). The twin boundary was clearly observed (indicated by the red dashed line in Fig. 5f). The directions of c-axes of $L1_0$-CoPt with twin planes at the top-edge and the nanowire–substrate interface are indicated as white and green arrows in Fig. 5e and f.

The TEM images, HAADF-STEM images, and NED pattern, which were observed from parallel to the nanowire-axis along the [110] zone axis, are shown in Fig. 6. From the BF-TEM image (Fig. 6a), even though the height of $L1_0$-CoPt nanowire varied in the range of 25–40 nm, Plateau–Rayleigh instability was well suppressed and the nanowire structure maintained after annealing. The annealed nanowires consisted of a chain of multidomain grains (Fig. 6a). The NED pattern (Fig. 6c) at the center of the grain showed superlattice diffraction spots of $L1_0$-CoPt *001* and *110* (indicated by the red circles) along with the fundamental spots (indicated by the yellow circles), which indicates nanostructure-induced $L1_0$-ordering of the CoPt nanowires after annealing. Furthermore, the HAADF-STEM image (Fig. 6d) showed alternating monoatomic layers of Co (appeared as dark spots and indicated by the light blue dots) and Pt (appeared as bright spots and indicated by the orange dots), where the c-axis of $L1_0$-CoPt was tilted with respect to the substrate normal. Twins with (110) twin planes were also clearly observed; the twin boundary is indicated by the red dashed lines in Fig. 6d.

The experimental results obtained from SEM, GI-XRD, VSM, NED, and TEM show the nanostructure-induced $L1_0$-ordering of twinned single-crystals in CoPt ferromagnetic nanowires, with a linewidth of approximately 30 nm and a large H_c over 10 kOe on Si/SiO_2 substrates by a lift-off process that combines of EBL and EB evaporation, followed by annealing.

The BF-TEM images clearly showed that the CoPt nanowires consisted of a chain of grains (Fig. 6a). From the cross-sectional HAADF-STEM images, $L1_0$-CoPt with alternating monoatomic layers of Co and Pt was observed at both the top-edge and near the nanowire–substrate interface of the nanowires from the nanowire-axis direction (Fig. 5e and f), respectively, and was also observed from parallel to the nanowire-axis (Fig. 6d). The twin planes were clearly observed in Fig. 5f and 6d. Because the NED patterns were taken at the grain slightly near the

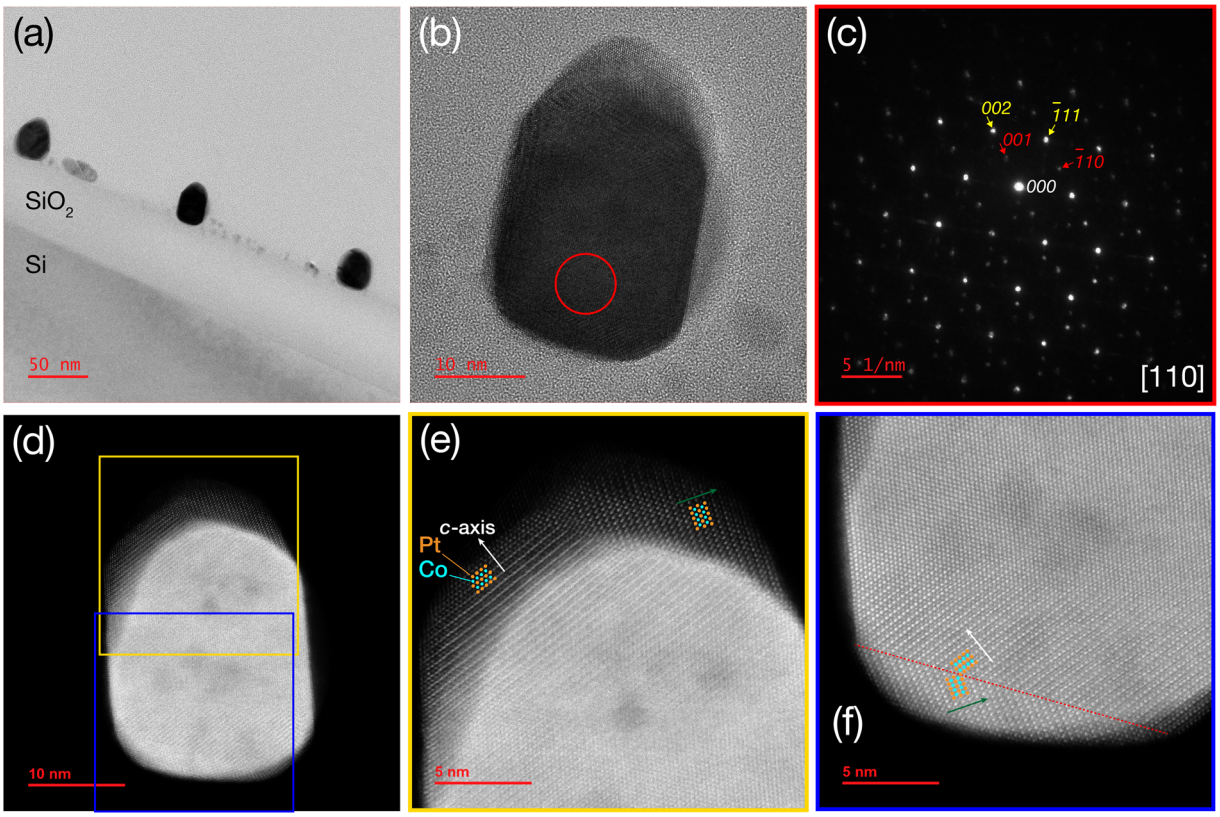

Fig. 5 Cross-sectional (a) bright field (BF)-TEM image, (b) magnified BF-TEM image, (c) nano-beam electron diffraction (NED) pattern, taken at the red circle in part (b), (d) high-angle annular dark field (HAADF)-scanning transmission electron microscope (STEM) image, and (e and f) magnified HAADF-STEM images of part (d) [(orange square for part (e) and red square for part (f))] of $(Co/Pt)_6$ nanowires on Si/SiO_2 substrates after annealing at 650 °C for 90 min, which were observed from the nanowire-axis direction along the [110] zone axis. In part (c), the superlattice diffraction spots of $L1_0$-CoPt are indicated by the red arrows, whereas the fundamental spots are indicated by the yellow arrows. In parts (e) and (f), Co and Pt atoms are indicated by the light blue and orange dots, respectively, and the directions of *c*-axes of $L1_0$-CoPt are shown as white and green arrows. The twin boundary is indicated by red dashed line in part (f).

nanowire–substrate interface (Fig. 5c) and at the center of the grain (Fig. 6c), and the CoPt nanowires with a linewidth of approximately 30 nm possessed not an $A1@L1_0$ core–shell but an entirely $L1_0$-ordered structure. As the directions of *c*-axes of $L1_0$-CoPt at the top-edge (white and green arrows in Fig. 5e) were the same as those at the nanowire–substrate interface (white and green arrows in Fig. 5f), respectively, the grain should be composed of single-crystals with twin boundaries. Consequently, "nanostructure-induced $L1_0$-ordering" of twinned single-crystals in CoPt ferromagnetic nanowires with a 30 nm scale ultrafine linewidth on Si/SiO_2 substrates were fabricated by EBL and annealing.

Here, we discuss the mechanism for nanostructure-induced $L1_0$-ordering of twinned single-crystals in CoPt ferromagnetic nanowires on Si/SiO_2 substrates based on (i) the atomic surface diffusion at the top-edge of the nanowires and (ii) the extremely large internal stress near the nanowire–substrate interface, originating from the 10 nm-curvature of the nanowires. When the $(Co/Pt)_6$ multilayer nanowires were subjected to annealing, Co and Pt atoms diffused on the nanowire surface and inter-diffused inside the nanowires, leading to form *A*1-disordered CoPt alloy nanowires. Considering the initial total thickness (50.4 nm) and the linewidth (30 nm) of the as-fabricated $(Co/Pt)_6$ multilayer nanowires, the initial cross-sectional aspect ratio (height-to-linewidth) of the nanowires was approximately 1.7, which is larger than unity. Thus, Co and Pt atoms at the top-edge of the nanowires diffused towards the sidewall of the nanowire surface so as to minimize the surface free energy. Owing to the extremely large internal stress at the 10 nm-curvature of the nanowires, the surface-diffused Co and Pt atoms began to form $L1_0$-CoPt nuclei possessing alternating monoatomic layers of Co and Pt, where the *c*-axis of $L1_0$-CoPt tended to be oriented normal direction to the curved nanowire surface, which is supported by the HAADF-STEM images (Fig. 5e and 6d). As the nanostructure-induced $L1_0$-ordering proceeded, the $L1_0$-ordering initiated at the nanowire surface progressed both laterally along the curved nanowire surface and towards the core of the nanowires. On the other hand, near the nanowire–substrate interface, extremely large internal stress is also generated perpendicular to the side of the nanowires (transverse direction with respect to the substrate normal), which is inversely proportional to the 10 nm-scale curvature radii and proportional to the surface tension, according to the Young–Laplace equation (eqn (1)). As a result, driving forces for

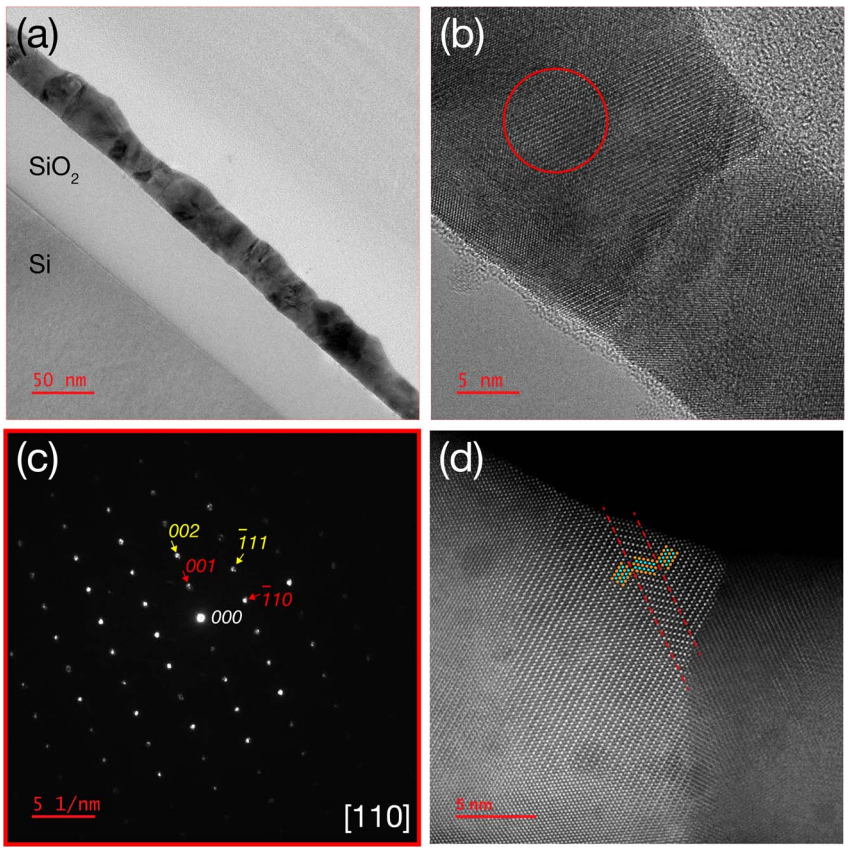

Fig. 6 Cross-sectional (a) BF-TEM image, (b) magnified BF-TEM image, (c) NED pattern, taken at the red circle in part (b), and (d) HAADF-STEM image of $(Co/Pt)_6$ nanowires on Si/SiO_2 substrates after annealing at 650 °C for 90 min, which were observed from parallel to the nanowire-axis along the [110] zone axis. In part (c), the superlattice diffraction spots of $L1_0$-CoPt are indicated by the red arrows, whereas the fundamental spots are indicated by the yellow arrows. In part (d), Co and Pt atoms are indicated by the light blue and orange dots, respectively. The twin boundaries are indicated by red dashed lines in part (d).

nanostructure-induced $L1_0$-ordering should be the atomic surface diffusion and extremely large internal stress, which lead the elliptical cross-sectional shapes of the nanowires with reduced heights in the BF-TEM images (Fig. 5a and b and 6a). Owing to these driving forces of atomic surface diffusion and extremely large internal stress, the $L1_0$-CoPt nuclei grow at the surface and toward the core of the grains in nanowires. The perturbation of the linewidth of the annealed CoPt nanowires was observed from the SEM image (Fig. 1b), which also supports the proposed driving forces for nanostructure-induced $L1_0$-ordering of twinned single-crystals in CoPt ferromagnetic nanowires.

Within the $L1_0$-CoPt grains, twin planes tended to be observed in the HAADF-STEM images (Fig. 5f and 6d). As the nanostructure-induced $L1_0$-ordering proceeded, $L1_0$-ordered CoPt grains impinged on the neighboring ones, leading to produce $L1_0$-ordered single-crystal grains with twin planes. Finally, the CoPt grains were entirely $L1_0$-ordered and the nanowires consisted of a chain of $L1_0$-ordered twinned single-crystals.

As the *c*-axis orientation of $L1_0$-ordered CoPt single-crystal grains differed between the grains, the superlattice peaks of $L1_0$-CoPt *001* and *110* exhibited Debye–Scherrer ring shapes in the 2D GI-XRD pattern (Fig. 2), which indicates that the *c*-axis of $L1_0$-CoPt was randomly tilted with respect to the substrate normal.

Nanostructure-induced $L1_0$-ordered CoPt ferromagnetic nanowires showed an identical H_c value of 10 kOe for the perpendicular, longitudinal, and transversal directions in the VSM results (Fig. 4). The direction of easy-axis of magnetization of nanowire structures tends to align along the wire-axis due to shape anisotropy.[92] The identical H_c value for the three measured directions of the CoPt nanowires in this study should be attributed to the different directions of easy-axis of magnetization in $L1_0$-ordered CoPt ferromagnetic twinned single-crystals.[93,94]

From the *M*–*H* curves in Fig. 4, a magnetic anisotropy field for the longitudinal direction (red curve) was larger than that for transversal (blue curve) and perpendicular (black curve) directions. Because the nanowires consisted of a chain of $L1_0$-ordered CoPt ferromagnetic twinned single-crystals, these grains had different directions of easy-axis of magnetization. As a result, the magnetic moment tended to be fluctuated by the neighboring grains, which leads to the larger anisotropy field for the longitudinal direction.

The nanostructure-induced $L1_0$-ordering of CoPt nanowires was confirmed at an annealing temperature of 650 °C, where the ordering temperature was lower than that for CoPt films with a large H_c over 10 kOe in our previous study (800 °C).[52] The decrease in the nanostructure-induced $L1_0$-ordering temperature was attributed to the melting point depression owing to the nanoscale structures,[95–106] which leads to nanostructure-induced $L1_0$-ordering of CoPt nanowires at lower ordering temperatures compared to that of the thin film structures.

The annealing temperature of 650 °C should be slightly higher than the process temperatures of Si technology. However, if the nanostructure-induced $L1_0$-ordering process will be introduced at first and followed usual Si technology processes, the nanostructure-induced $L1_0$-ordering process could be used.

As mentioned in the Introduction part, $L1_0$-ordered ferromagnetic nanowires have been typically fabricated by means of etching and electrodeposition.[43,60–73] However, the fabrication method of our nanostructure-induced $L1_0$-ordered ferromagnetic nanowires is different from those of the nanowires in the literature: compared to the nanowires fabricated by etching,[63] our nanowires do not require any etching process, which makes the fabrication process for spintronic devices less complicated. In addition, nanostructure-induced $L1_0$-ordering method could prepare $L1_0$-ordered ferromagnetic nanowires directly on Si/SiO_2 substrates without single-crystal substrates such as MgO. The electrodeposited nanowires also require anodized aluminum oxide templates, and tends to anneal higher temperature of 700–800 °C to obtain $L1_0$-ordered phase with high H_c.[64–73] Consequently, the nanostructure-induced $L1_0$-ordering method and the fabricated ferromagnetic nanowires have many advantageous towards future spintronic device application.

The ordering mechanism in nanostructured CoPt and FePt has been studied theoretically and experimentally in terms of free surface, surface segregation, surface diffusion, defect, size, and shape.[107–128] For example, $L1_0$-ordering has been found to proceed more quickly at the free surfaces than at the core of the nanostructures.[120,124] Surface segregation of Pt has been found to regulate the stoichiometry of the inner layers below the top surface, leading to affect the atomic ordering of the core of the nanostructures.[112,121] However, most of these studies have focused on the nanoparticles rather than nanowires on solid-state substrates. Thus, our experimental demonstration and proposed mechanism for nanostructure-induced $L1_0$-ordering of CoPt ferromagnetic nanowires on Si/SiO_2 substrates at the 10 nm-curvature of the nanowires would give an alternative insight into the nanoscale ordering behaviors.

Consequently, we demonstrated the nanostructure-induced $L1_0$-ordering method for fabricating twinned single-crystals in CoPt ferromagnetic nanowires with a linewidth of approximately 30 nm on Si/SiO_2 substrates by a lift-off process combining EBL and EB evaporation, followed by annealing, which exhibited a large H_c over 10 kOe. The realization of the CoPt ferromagnetic nanowires through nanostructure-induced $L1_0$-ordering would provide an alternative method for manufacturing nanoscale spintronic devices on Si/SiO_2 substrates. The nanostructure-induced $L1_0$-ordering would also offer another $L1_0$-ordering route of nanoscale ferromagnetic alloys. The concept of nanostructure-induced $L1_0$-ordering could also be applied to other $L1_0$-ordered ferromagnetic materials, such as FePt,[30,32] FePd,[129] CoPd,[130] and precious-metal-free FeNi[131] and FeCo.[132–134] Furthermore, our approach could be applied to other types of materials, leading to emergence of material properties different form their bulk ones, which is driven by the nanostructure itself. This will potentially open up a research field on "nanostructure-induced materials science and engineering".

3. Conclusions

We demonstrated nanostructure-induced $L1_0$-ordering method for fabricating twinned single-crystals in CoPt ferromagnetic nanowires with a 30 nm scale ultrafine linewidth on Si/SiO_2 substrates. The ultrasmall 10 nm scale curvature of the nanowires induced $L1_0$-ordering, wherein the driving forces were the atomic interdiffusion, surface diffusion, and extremely large internal stress during annealing. $(Co/Pt)_6$ multilayer nanowires were fabricated on Si/SiO_2 substrates by a lift-off process combining EBL and EB evaporation, followed by annealing at 650 °C for 90 min under a hydrogen atmosphere. The nanostructure-induced $L1_0$-ordering of CoPt ferromagnetic nanowires was confirmed by the experimental results obtained from SEM, GI-XRD, VSM, and TEM. The nanostructure-induced $L1_0$-ordered CoPt ferromagnetic nanowires showed a linewidth of approximately 30 nm, exhibiting an identical large H_c of 10 kOe for the perpendicular, longitudinal, and transversal directions. The identical H_c value for the three measured directions of the CoPt nanowires corresponded to the different directions of easy-axis of magnetization in $L1_0$-ordered CoPt ferromagnetic twinned single-crystals, as evident in the superlattice peaks of $L1_0$-CoPt *001* and *110* with Debye–Scherrer ring shapes. The cross-sectional STEM images observed from the nanowire-axis direction and parallel to the nanowire-axis and the NED patterns revealed $L1_0$-ordered CoPt single-crystals with twin planes. Furthermore, we discussed the mechanism for nanostructure-induced $L1_0$-ordering of CoPt ferromagnetic nanowires on Si/SiO_2 substrates based on (i) the atomic surface diffusion at the top-edge of the nanowires and (ii) the extremely large internal stress near the nanowire–substrate interface, originating from the 10 nm-curvature of the nanowires. Our proof-of-concept demonstration of nanostructure-induced $L1_0$-ordering of twinned single-crystals in CoPt ferromagnetic nanowires on Si/SiO_2 substrates would be significant for realizing silicon-technology-based CMOS-compatible non-volatile spintronic nanodevices in the future.

4. Experimental section

4.1. Fabrication

CoPt ferromagnetic nanowires were fabricated by a lift-off process combining EBL and EB evaporation. An EB resist (ZEP520A, Zeon) diluted with anisole (ZEP-A, Zeon) was coated on cleaned Si(100) (525 μm)/SiO_2 (50 nm) substrates by a spin

coater, followed by pre-baking on a hot plate. The nanowire structures with an interval of ~100 nm were patterned on the resist-coated substrates by an EBL apparatus (ELS-7500EX, Elionix) with dimensions of approximately 5 mm × 3 mm. Then, $[Co\ (3.6\ nm)/Pt\ (4.8\ nm)]_6$ multilayer was deposited on the developed samples by EB evaporation. The deposited samples were then lifted-off. The fabricated $(Co/Pt)_6$ nanowires were subsequently annealed at 650 °C for 30–90 min under a flowing Ar/H_2 (3%) mixed gas atmosphere using an RTA apparatus (MILA-5000UHV, Advance Riko).

4.2. Characterization

The surface morphologies of the nanowires were observed using an SEM (SU8000 and Regulus8230, Hitachi High-Tech). The crystal structures of the nanowires were characterized by GI-XRD method using the synchrotron radiation at the BL-8B line of the Photon Factory, High Energy Accelerator Research Organization (KEK), Japan.[50–52] The measurements were performed using an X-ray diffractometer (R-Axis, Rigaku). A monochromic synchrotron X-ray beam at a wavelength of 1.05303 Å was irradiated onto the sample with grazing incidence angles. During the exposure, the sample was oscillated with 1.2°–3.2° range. The 2D GI-XRD patterns were collected by a curved imaging plate. To eliminate the background signal from the substrates, 2D GI-XRD patterns for the substrates were also measured with the same measurement geometry as that for the nanowires. To quantitatively evaluate the diffraction peaks derived from $L1_0$-CoPt, the intensity–2θ 1D GI-XRD profiles of the nanowires were obtained from the 2D GI-XRD patterns using instrument software (Display, Rigaku). Each of the experimental superlattice peaks of $L1_0$-CoPt was analyzed with a bell-shaped function after subtracting the remaining background signal.[52] The lattice parameters (c and a) for $L1_0$-CoPt were obtained from the superlattice peaks of $L1_0$-CoPt *001* and *110*, respectively. The diffraction peaks were assigned using the powder diffraction file (PDF) card (CoPt: 03-065-8969) and ref. 135. A superconducting quantum interference device VSM (MPMS3, Quantum Design) was used to measure M–H curves of the nanowires. Three M–H curves were measured by applying a maximum external magnetic field of 70 kOe in the following directions: out-of-plane direction (perpendicular), in-plane direction parallel to the nanowire-axis (longitudinal), and in-plane direction perpendicular to the nanowire-axis (transversal). The M–H curves were measured in a vacuum at room temperature (27 °C). After the characterization by SEM, GI-XRD, and VSM, TEM samples were prepared by a focused ion beam. Cross-sectional BF-TEM images, HAADF-STEM images, and NED patterns of the nanowires were observed and analyzed by a TEM (JEM-ARM200F "NEOARM", JEOL), which were taken from both the nanowire-axis direction and parallel to the nanowire-axis along the [110] zone axis.

Conflicts of interest

There are no conflicts to declare.

Acknowledgements

We thank Michiyo Miyakawa for the technical support with the SEM measurements. This study was partially supported by the MEXT Element Strategy Initiative to Form Core Research Centers (Grant No. JPMXP0112101001). The synchrotron XRD experiment was performed with the approval of the Photon Factory Program Advisory Committee (Proposal No. 2016S2004, 2019V003, 2019G534, and 2021G635). R. T. acknowledges JSPS DC2 fellowship (Grant No. 21J13665).

References

1 S. S. P. Parkin, M. Hayashi and L. Thomas, *Science*, 2008, **320**, 190–194.
2 S. Parkin and S.-H. Yang, *Nat. Nanotechnol.*, 2015, **10**, 195–198.
3 J.-E. Wegrowe, D. Kelly, Y. Jaccard, P. Guittienne and J.-P. Ansermet, *Europhys. Lett.*, 1999, **45**, 626–632.
4 N. Vernier, D. A. Allwood, D. Atkinson, M. D. Cooke and R. P. Cowburn, *Europhys. Lett.*, 2004, **65**, 526–532.
5 T. Koyama, D. Chiba, K. Ueda, K. Kondou, H. Tanigawa, S. Fukami, T. Suzuki, N. Ohshima, N. Ishiwata, Y. Nakatani, K. Kobayashi and T. Ono, *Nat. Mater.*, 2011, **10**, 194–197.
6 S. Fukami, T. Suzuki, Y. Nakatani, N. Ishiwata, M. Yamanouchi, S. Ikeda, N. Kasai and H. Ohno, *Appl. Phys. Lett.*, 2011, **98**, 082504.
7 T. Thurn-Albrecht, J. Schotter, G. A. Kästle, N. Emley, T. Shibauchi, L. Krusin-Elbaum, K. Guarini, C. T. Black, M. T. Tuominen and T. P. Russell, *Science*, 2000, **290**, 2126–2129.
8 S. Z. Chu, S. Inoue, K. Wada and K. Kurashima, *Electrochim. Acta*, 2005, **51**, 820–826.
9 X. Kou, X. Fan, R. K. Dumas, Q. Lu, Y. Zhang, H. Zhu, X. Zhang, K. Liu and J. Q. Xiao, *Adv. Mater.*, 2011, **23**, 1393–1397.
10 L. Piraux, J. M. George, J. F. Despres, C. Leroy, E. Ferain, R. Legras, K. Ounadjela and A. Fert, *Appl. Phys. Lett.*, 1994, **65**, 2484–2486.
11 A. Blondel, J. P. Meier, B. Doudin and J.-P. Ansermet, *Appl. Phys. Lett.*, 1994, **65**, 3019–3021.
12 K. Liu, K. Nagodawithana, P. C. Searson and C. L. Chien, *Phys. Rev. B*, 1995, **51**, 7381–7384.
13 A. Fert and L. Piraux, *J. Magn. Magn. Mater.*, 1999, **200**, 338–358.
14 Z.-M. Liao, Y.-D. Li, J. Xu, J.-M. Zhang, K. Xia and D.-P. Yu, *Nano Lett.*, 2006, **6**, 1087–1091.
15 L. Piraux, K. Renard, R. Guillemet, S. Mátéfi-Tempfli, M. Mátéfi-Tempfli, V. A. Antohe, S. Fusil, K. Bouzehouane and V. Cros, *Nano Lett.*, 2007, **7**, 2563–2567.
16 K. T. Chan, C. Doran, E. G. Shipton and E. E. Fullerton, *IEEE Trans. Magn.*, 2010, **46**, 2209–2211.
17 G. Muscas, P. E. Jönsson, I. G. Serrano, Ö. Vallin and M. V. Kamalakar, *Nanoscale*, 2021, **13**, 6043–6052.
18 Z. Duan, A. Smith, L. Yang, B. Youngblood, J. Lindner, V. E. Demidov, S. O. Demokritov and I. N. Krivorotov, *Nat. Commun.*, 2014, **5**, 5616.

19 C. Safranski, E. Montoya and I. N. Krivorotov, *Nat. Nanotechnol.*, 2019, **14**, 27–30.
20 Z. K. Wang, M. H. Kuok, S. C. Ng, D. J. Lockwood, M. G. Cottam, K. Nielsch, R. B. Wehrspohn and U. Gösele, *Phys. Rev. Lett.*, 2002, **98**, 027201.
21 C. Liu, J. Chen, T. Liu, F. Heimbach, H. Yu, Y. Xiao, J. Hu, M. Liu, H. Chang, T. Stueckier, S. Tu, Y. Zhang, Y. Zhang, P. Gao, Z. Liao, D. Yu, K. Xia, N. Lei, W. Zhao and M. Wu, *Nat. Commun.*, 2018, **9**, 738.
22 Y. Yamane, J. Ieda and S. Maekawa, *Appl. Phys. Lett.*, 2012, **100**, 162401.
23 M. Hayashi, J. Ieda, Y. Yamane, J. Ohe, Y. K. Takahashi, S. Mitani and S. Maekawa, *Phys. Rev. Lett.*, 2012, **108**, 147202.
24 A. Mukhtar, K. Wu, X. Cao and L. Gu, *Nanotechnology*, 2020, **31**, 433001.
25 M. Tanase, E. J. Felton, D. S. Gray, A. Hultgren, C. S. Chen and D. H. Reich, *Lab Chip*, 2005, **5**, 598–605.
26 D. Weller and A. Moser, *IEEE Trans. Magn.*, 1999, **35**, 4423–4439.
27 D. Weller, A. Moser, L. Folks, M. E. Best, W. Lee, M. F. Toney, M. Schwickert, J.-U. Thiele and M. F. Doerner, *IEEE Trans. Magn.*, 2000, **36**, 10–15.
28 S. H. Liou, Y. Liu, S. S. Malhotra, M. Yu and D. J. Sellmyer, *J. Appl. Phys.*, 1996, **79**, 5060–5062.
29 S. H. Liou, S. Huang, E. Klimek, R. D. Kirby and Y. D. Yao, *J. Appl. Phys.*, 1999, **85**, 4334–4336.
30 R. A. Ristau, K. Barmak, L. H. Lewis, K. R. Coffey and J. K. Howard, *J. Appl. Phys.*, 1999, **86**, 4527–4533.
31 P. Andreazza, V. Pierron-Bohnes, F. Tournus, C. Andreazza-Vignolle and V. Dupuis, *Surf. Sci. Rep.*, 2015, **70**, 188–258.
32 K. Barmak, J. Kim, L. H. Lewis, K. R. Coffey, M. F. Toney, A. J. Kellock and J.-U. Thiele, *J. Appl. Phys.*, 2005, **98**, 033904.
33 R. K. Rakshit, S. K. Bose, R. Sharma, R. C. Budhani, T. Vijaykumar, S. J. Neena and G. U. Kulkarni, *J. Appl. Phys.*, 2008, **103**, 023915.
34 H. Zeng, M. L. Yan, N. Powers and D. J. Sellmyer, *Appl. Phys. Lett.*, 2002, **80**, 2350–2352.
35 S. C. Chen, S. P. Chen and P. C. Kuo, *Thin Solid Films*, 2009, **517**, 5176–5180.
36 T. Narisawa, T. Hasegawa, S. Ishio and H. Yamane, *J. Appl. Phys.*, 2011, **109**, 033918.
37 S. N. Hsiao, S. H. Liu, S. K. Chen, T. S. Chin and H. Y. Lee, *Appl. Phys. Lett.*, 2012, **100**, 261909.
38 L.-W. Wang, W.-C. Shih, Y.-C. Wu and C.-H. Lai, *Appl. Phys. Lett.*, 2012, **101**, 252403.
39 M. Mizuguchi, T. Sakurada, T. Y. Tashiro, K. Sato, T. J. Konno and K. Takanashi, *APL Mater.*, 2013, **1**, 032117.
40 T. Tashiro, M. Mizuguchi, T. Kojima, T. Koganezawa, M. Kotsugi, T. Ohtsuki, K. Sato, T. Konno and K. Takanashi, *J. Alloys Compd.*, 2018, **750**, 164–170.
41 M. L. Yan, N. Powers and D. J. Sellmyer, *J. Appl. Phys.*, 2003, **93**, 8292–8294.
42 J.-Y. Chiou, H. W. Chang, C.-C. Chi, C.-H. Hsiao and C. Ouyang, *ACS Appl. Nano Mater.*, 2019, **2**, 5663–5673.
43 J. W. Lau and J. M. Shaw, *J. Phys. D: Appl. Phys.*, 2011, **44**, 303001.
44 Y. Y. Choi, T. Teranishi and Y. Majima, *Appl. Phys. Express*, 2019, **12**, 025002.
45 Y. Y. Choi, A. Kwon and Y. Majima, *Appl. Phys. Express*, 2019, **12**, 125003.
46 S. J. Lee, J. Kim, T. Tsuda, R. Takano, R. Shintani, K. Nozaki and Y. Majima, *Appl. Phys. Express*, 2019, **12**, 125007.
47 M. Yang, R. Toyama, P. T. Tue and Y. Majima, *Appl. Phys. Express*, 2020, **13**, 015006.
48 P. T. Tue, T. Tosa and Y. Majima, *Sens. Actuators, B*, 2021, **343**, 130098.
49 P.-C. Yeh, G. Ohkatsu, R. Toyama, P. T. Tue, K. K. Ostrikov, Y. Majima and W.-H. Chiang, *Nanotechnology*, 2021, **32**, 50LT01.
50 R. Toyama, S. Kawachi, S. Iimura, J. Yamaura, Y. Murakami, H. Hosono and Y. Majima, *Mater. Res. Express*, 2020, **7**, 066101.
51 R. Toyama, S. Kawachi, J. Yamaura, Y. Murakami, H. Hosono and Y. Majima, *Jpn. J. Appl. Phys.*, 2020, **59**, 075504.
52 R. Toyama, S. Kawachi, J. Yamaura, Y. Murakami, H. Hosono and Y. Majima, *Jpn. J. Appl. Phys.*, 2022, **61**, 065002.
53 A. Makarov, T. Windbacher, V. Sverdlov and S. Selberherr, *Semicond. Sci. Technol.*, 2016, **31**, 113006.
54 J. Ender, S. Fiorentini, R. L. D. Orio, W. Goes, V. Sverdlov and S. Selberherr, *IEEE J. Electron Devices Soc.*, 2021, **9**, 456–463.
55 K. Yakushiji, S. Mitani, F. Ernult, K. Takanashi and H. Fujimori, *Phys. Rep.*, 2007, **451**, 1–35.
56 P. Seneor, A. Bernand-Mantel and F. Petroff, *J. Phys.: Condens. Matter*, 2007, **19**, 165222.
57 J. Barnaś and I. Weymann, *J. Phys.: Condens. Matter*, 2008, **20**, 423202.
58 K. J. Dempsey, D. Ciudad and C. H. Marrows, *Philos. Trans. R. Soc., A*, 2011, **369**, 3150–3174.
59 A. Hirohata and K. Takanashi, *J. Phys. D: Appl. Phys.*, 2014, **47**, 193001.
60 M. S. Wei and S. Y. Chou, *J. Appl. Phys.*, 1994, **76**, 6679–6681.
61 B. Leven, U. Nowak and G. Dumpich, *Europhys. Lett.*, 2005, **70**, 803–809.
62 A. Fernández-Pacheco, J. M. De Teresa, R. Córdoba and M. R. Ibarra, *J. Phys. D: Appl. Phys.*, 2009, **42**, 055005.
63 V. D. Nguyen, L. Vila, A. Marty, J. C. Pillet, L. Notin, C. Beigné, S. Pizzini and J. P. Attané, *Appl. Phys. Lett.*, 2012, **100**, 252403.
64 Y. H. Huang, H. Okumura, G. C. Hadjipanayis and D. Weller, *J. Appl. Phys.*, 2002, **91**, 6869–6871.
65 N. Yasui, A. Imada and T. Den, *Appl. Phys. Lett.*, 2003, **83**, 3347–3349.
66 J. Mallet, K. Yu-Zhang, S. Mátéfi-Tempfli, M. Mátéfi-Tempfli and L. Piraux, *J. Phys. D: Appl. Phys.*, 2005, **38**, 909–914.
67 F. M. F. Rhen, E. Backen and J. M. D. Coey, *J. Appl. Phys.*, 2005, **97**, 113908.
68 Y. Dahmane, L. Cagnon, J. Voiron, S. Pairis, M. Bacia, L. Ortega, N. Benbrahim and A. Kadri, *J. Phys. D: Appl. Phys.*, 2006, **39**, 4523–4528.

69 A. I. Gapin, X. R. Ye, J. F. Aubuchon, L. H. Chen, Y. J. Tang and S. Jin, *J. Appl. Phys.*, 2006, **99**, 08G902.
70 L. Cagnon, Y. Dahmane, J. Voiron, S. Pairis, M. Bacia, L. Ortega, N. Benbrahim and A. Kadri, *J. Magn. Magn. Mater.*, 2007, **310**, 2428–2430.
71 A. I. Gapin, X.-R. Ye, L.-H. Chen, D. Hong and S. Jin, *IEEE Trans. Magn.*, 2007, **43**, 2151–2153.
72 L.-F. Liu, S.-S. Xie and W.-Y. Zhou, *J. Phys. D: Appl. Phys.*, 2009, **42**, 205002.
73 F. N. Byrne, L. M. A. Monzon, P. Stamenov, M. Venkatesan and J. M. D. Coey, *Appl. Phys. Lett.*, 2011, **98**, 252507.
74 J. S. Rowlinson and B. Widom, *Molecular Theory of Capillarity*, Clarendon Press, Oxford University Press, Oxford, 1982.
75 J. W. van Honschoten, N. Brunets and N. R. Tas, *Chem. Soc. Rev.*, 2010, **39**, 1096–1114.
76 H. Liu and G. Cao, *Sci. Rep.*, 2016, **6**, 23936.
77 M. E. Toimil-Molares, A. G. Balogh, T. W. Cornelius, R. Neumann and C. Trautmann, *Appl. Phys. Lett.*, 2004, **85**, 5337–5339.
78 S. Karim, M. E. Toimil-Molares, A. G. Balogh, W. Ensinger, T. W. Cornelius, E. U. Khan and R. Neumann, *Nanotechnology*, 2006, **17**, 5954–5959.
79 J. Petersen and S. G. Mayr, *J. Appl. Phys.*, 2008, **103**, 023520.
80 H. Li, J. M. Biser, J. T. Perkins, S. Dutta, R. P. Vinci and H. M. Chan, *J. Appl. Phys.*, 2008, **103**, 024315.
81 Z. F. Zhou, Y. Pan, Y. C. Zhou and L. Yang, *Appl. Surf. Sci.*, 2011, **257**, 9991–9995.
82 M. Rauber, F. Muench, M. E. Toimil-Molares and W. Ensinger, *Nanotechnology*, 2012, **23**, 475710.
83 R. W. Day, M. N. Mankin, R. Gao, Y.-S. No, S.-K. Kim, D. C. Bell, H.-G. Park and C. M. Lieber, *Nat. Nanotechnol.*, 2015, **10**, 345–352.
84 S. Vigonski, V. Jansson, S. Vlassov, B. Polyakov, E. Baibuz, S. Oras, A. Aabloo, F. Djurabekova and V. Zadin, *Nanotechnology*, 2018, **29**, 015704.
85 J. Plateau, *Transl. Annual Reports of the Smithsonian Institution*, Vol. 1863, 1873.
86 L. Rayleigh, *Proc. Lond. Math. Soc.*, 1878, **10**, 4–13.
87 L. Rayleigh, *Proc. R. Soc. London*, 1879, **29**, 71–97.
88 J. Eggers, *Rev. Mod. Phys.*, 1997, **69**, 865–929.
89 F. A. Nichols and W. W. Mullins, *J. Appl. Phys.*, 1965, **36**, 1826–1835.
90 F. A. Nichols, *J. Mater. Sci.*, 1976, **11**, 1077–1082.
91 Y. Wang, X. Zhang, Y. Liu, Y. Jiang, Y. Zhang, J. Wang, Y. Liu, H. Liu, Y. Sun, G. S. D. Beach and J. Yang, *J. Phys. D: Appl. Phys.*, 2012, **45**, 485001.
92 D. J. Sellmyer, M. Zheng and R. Skomski, *J. Phys.: Condens. Matter*, 2001, **13**, R433–R460.
93 A.-C. Sun, F.-T. Yuan, J.-H. Hsu and H. Y. Lee, *Scr. Mater.*, 2009, **61**, 713–716.
94 F.-T. Yuan, A.-C. Sun, C. F. Huang and J.-H. Hsu, *Nanotechnology*, 2014, **25**, 165601.
95 C. R. M. Wronski, *Br. J. Appl. Phys.*, 1967, **18**, 1731–1737.
96 Ph. Buffat and J.-P. Borel, *Phys. Rev. A*, 1976, **13**, 2287–2298.
97 T. Ben David, Y. Lereah, G. Deutscher, R. Kofman and P. Cheyssac, *Philos. Mag. A*, 1995, **71**, 1135–1143.
98 O. Gulseren, F. Ercolessi and E. Tosatti, *Phys. Rev. B*, 1995, **51**, 7377–7380.
99 S. L. Lai, J. Y. Guo, V. Petrova, G. Ramanath and L. H. Allen, *Phys. Rev. Lett.*, 1996, **77**, 99–102.
100 M. Zhang, M. Y. Efremov, F. Schiettekatte, E. A. Olson, A. T. Kwan, S. L. Lai, T. Wisleder, J. E. Greene and L. H. Allen, *Phys. Rev. B*, 2000, **62**, 10548–10557.
101 L. Miao, V. R. Bhethanabotla and B. Joseph, *Phys. Rev. B*, 2005, **72**, 134109.
102 W. H. Qi, *Physica B*, 2005, **368**, 46–50.
103 G. Abudukelimu, G. Guisbiers and M. Wautelet, *J. Mater. Res.*, 2006, **21**, 2829–2834.
104 H. S. Shin, J. Yu and J. Y. Song, *Appl. Phys. Lett.*, 2007, **91**, 173106.
105 W. Luo, W. Hu and S. Xiao, *J. Chem. Phys.*, 2008, **128**, 074710.
106 A. van Teijlingen, S. A. Davis and S. R. Hall, *Nanoscale Adv.*, 2020, **2**, 2347–2351.
107 M. Polak and L. Rubinovich, *Surf. Sci. Rep.*, 2000, **38**, 127–194.
108 T. J. Klemmer, C. Liu, N. Shukla, X. W. Wu, D. Weller, M. Tanase, D. E. Laughlin and W. A. Soffa, *J. Magn. Magn. Mater.*, 2003, **266**, 79–87.
109 Y. K. Takahashi, T. Koyama, M. Ohnuma, T. Ohkubo and K. Hono, *J. Appl. Phys.*, 2004, **95**, 2690–2696.
110 M. Kozłowski, R. Kozubski, V. Pierron-Bohnes and W. Pfeiler, *Comput. Mater. Sci.*, 2005, **33**, 287–295.
111 B. Yang, M. Asta, O. N. Mryasov, T. J. Klemmer and R. W. Chantrell, *Scr. Mater.*, 2005, **53**, 417–422.
112 M. Müller and K. Albe, *Phys. Rev. B*, 2005, **72**, 094203.
113 B. Yang, M. Asta, O. N. Mryasov, T. J. Klemmer and R. W. Chantrell, *Acta Mater.*, 2006, **54**, 4201–4211.
114 G. Rossi, R. Ferrando and C. Mottet, *Faraday Discuss.*, 2008, **138**, 193–210.
115 J. Penuelas, C. Andreazza-Vignolle, P. Andreazza, A. Ouerghi and N. Bouet, *Surf. Sci.*, 2008, **602**, 545–551.
116 D. Alloyeau, C. Ricolleau, C. Mottet, T. Oikawa, C. Langlois, Y. Le Bouar, N. Braidy and A. Loiseau, *Nat. Mater.*, 2009, **8**, 940–946.
117 H. M. Chen, C. F. Hsin, P. Y. Chen, R.-S. Liu, S.-F. Hu, C.-Y. Huang, J.-F. Lee and L.-Y. Jang, *J. Am. Chem. Soc.*, 2009, **131**, 15794–15801.
118 R. V. Chepulskii, W. H. Butler, A. van de Walle and S. Curtarolo, *Scr. Mater.*, 2010, **62**, 179–182.
119 M. E. Gruner, *J. Phys.: Conf. Ser.*, 2010, **200**, 072039.
120 M. Müller and K. Albe, *Beilstein J. Nanotechnol.*, 2011, **2**, 40–46.
121 R. V. Chepulskii and W. H. Butler, *Phys. Rev. B*, 2012, **86**, 155401.
122 S. Yamakawa, R. Asahi and T. Koyama, *Mater. Trans.*, 2013, **54**, 1242–1249.
123 A. Lopes, G. Tréglia, C. Mottet and B. Legrand, *Phys. Rev. B*, 2015, **91**, 035407.
124 S. Brodacka, M. Kozlowski, R. Kozubski, Ch. Goyhenex and G. E. Murch, *Phys. Chem. Chem. Phys.*, 2015, **17**, 28394–28406.

125 S. Dai, Y. You, S. Zhang, W. Cai, M. Xu, L. Xie, R. Wu, G. W. Graham and X. Pan, *Nat. Commun.*, 2017, **8**, 204.
126 H. Sepehri-Amin, H. Iwama, G. Hrkac, K. T. Butler, T. Shima and K. Hono, *Scr. Mater.*, 2017, **135**, 88–91.
127 F. Li, Y. Zong, Y. Ma, M. Wang, W. Shang, P. Tao, C. Song, T. Deng, H. Zhu and J. Wu, *ACS Nano*, 2021, **15**, 5284–5293.
128 A. Front and C. Mottet, *J. Phys. Chem. C*, 2021, **125**, 16358–16365.
129 V. Gehanno, A. Marty, B. Gilles and Y. Samson, *Phys. Rev. B*, 1997, **55**, 12552–12555.
130 Y. Matsuo, *J. Phys. Soc. Jpn.*, 1972, **32**, 972–978.
131 M. Kotsugi, C. Mitsumata, H. Maruyama, T. Wakita, T. Taniuchi, K. Ono, M. Suzuki, N. Kawamura, N. Ishimatsu, M. Oshima, Y. Watanabe and M. Taniguchi, *Appl. Phys. Express*, 2010, **3**, 013001.
132 T. Burkert, L. Nordström, O. Eriksson and O. Heinonen, *Phys. Rev. Lett.*, 2004, **93**, 027203.
133 T. Hasegawa, S. Kanatani, M. Kazaana, K. Takahashi, K. Kumagai, M. Hirao and S. Ishio, *Sci. Rep.*, 2017, **7**, 13215.
134 H. Ito, M. Saito, T. Miyamachi, F. Komori, T. Koganezawa, M. Mizuguchi and M. Kotsugi, *AIP Adv.*, 2019, **9**, 045307.
135 W. B. Pearson, *A Handbook of Lattice Spacings and Structures of Metals and Alloys*, Pergamon Press, Oxford, 1958.